TASK QUARTERLY 6 No 1 (2002), 63–78

A NOVEL 3D INVERSE METHOD FOR THE DESIGN OF TURBOMACHINERY BLADES IN ROTATIONAL VISCOUS FLOW: THEORY AND APPLICATIONS

WEE TECK TIOW AND MEHRDAD ZANGENEH

Department of Mechanical Engineering,
University College London,
Torrington Place, WC1E 7JE London, United Kingdom
m_zangeneh@meng.ucl.ac.uk

(Received 16 August 2001)

Abstract: The development and application of a three-dimensional (3D) inverse methodology is presented for the design of turbomachinery blades. The design method is based on the specification of the blade loading distribution and the corresponding blade shape is systematically sought using directly the difference between the target and initial values. The design procedure comprises mainly of a CFD solver code and the blade-update algorithm to calculate the desired blade geometry as well as the corresponding 3D flow.

The CFD code is a well-validated three-dimensional flow solver and has shock capturing ability to cope in both subsonic and high transonic-shocked, viscous flow. Fundamentally, it is a cell-vertex, finite volume, time-marching solver employing the multistage Runge-Kutta integrator in conjunction with accelerating techniques (local time stepping and grid sequencing). To account for viscosity, viscous forces are included in the solution using the log-law and mixing length models. The effects of rotating blades as well as tip clearance flow are also included in the flow prediction.

The capabilities of the present method are demonstrated in the re-design of a transonic fan blade, the NASA Rotor 67. The re-design focuses on the shocked flow near the tip, where the effects of shock-boundary interaction and leakage flow are examined. The result shows conclusively that the shock-formation and its intensity in such a high-speed turbomachinery flow are well defined on the loading distributions. Simple guidelines to change the loading distribution can be followed using the proposed inverse methodology to improve the blade shape.

Keywords: inverse design, blade loading, turbomachinery, blades

Notation

N – number of blades in cascade arrangement
R – gas constant
rV_θ – swirl velocity
s – blade pitch
t_θ – tangential blade thickness (radian)
V – absolute velocity

$\alpha^{\pm}$ – angular offset of a point on the upper and lower, surfaces of a blade
ΔS – Generated Entropy
ω – rotational speed

Subscripts

bl – average flow values on the upper and lower blade surfaces

Superscripts

n – n^{th} design iteration
0 – initial value
1 – first approximation
$+$ – upper surface of a blade
$-$ – lower surface of a blade
$*$ – target value (used to denote the specified design value)

Overbars

$\sim$ – mass-average

1. Introduction

The advances of computational techniques in flow analysis have been tremendous in the last decade. Complemented by increasing computing power, it is now common to use a variety of three-dimensional Euler and Navier-Stokes solver codes for routine design [1]. Based on the CFD results, successive blade modifications are usually performed in order to achieve an ideal flow pattern. The conventional blade design practice is based on empirical methods combined with the experience of specialist designers. The progress depends greatly upon the designers' experience and can be laborious and expensive. Recently, radical new methods have emerged and their principles suggest that blade optimization may be achieved in a more theoretical and logical manner.

One new class of systematic design methods is usually referred to as *Inverse methodology*. In this approach, the blade geometry is computed directly from the specification of a required flow parameter. Existing 2D and 3D inverse methods are formulated with different design parameters. Three popular specifications are:

1. the surface static pressure [2–4],
2. surface static pressure difference between the blade upper and lower surface [5–7] and
3. averaged mean swirl (radius multiplied by tangential velocity, rV_{θ}) distribution throughout the meridional section of the machine [8–10].

Successful applications of the various inverse methods in the improvement of three-dimensional axial and radial blades have been reported [11] applied their method to various designs of compressor and turbine blades. The method of Zangeneh has been utilized in several practical attempts including the suppression of secondary flows in centrifugal impellers and diffusers [12, 13]; and recently, in improving the stage performance of a high-pressure pump [14] and LP turbine stage [15].

The success of the inverse design methodology in practical blade design has been its ability to allow designers to use their fluid dynamics insights directly to affect their design in the improvement process. The systematic approach taken by the inverse methods provide the important link between design intent and the blade geometry.

More sophisticated inverse methodologies now being developed are based on advanced CFD techniques. At the most advanced level, the method has shock capturing ability and can cope with both subsonic and transonic, viscous flow [16] reported an improved 2D method based on surface static pressure specification useful for the design of transonic compressor cascades in viscous flow. The theoretical development of three-dimensional methods based on the specification of static pressure loading has also been reported [17, 18]. The practical applications of this method have included transonic fan and compressor designs [19, 20] as well as for splitter blades [21].

In this article, the theory and application of another three-dimensional viscous transonic inverse method is presented. The current approach combines the use of an explicit time-marching flow solver with the design procedure based on mass-averaged swirl as suggested by Hawthorne [8]. The proposed method essentially solves the full 3D Euler equations and the design algorithm has been formulated to include the explicit specification of the blade tangential thickness and thus has the ability to cope with thick profiles. To account for viscosity, the inviscid solution has also been improved by adding a viscous loss simulation using the log-law and the mixing length models. The proposed design principle differs from the other viscous methods [16, 17, 20] where it is necessary to model the wall surface to be permeable using a mathematical transpiration model. In this method, the surface boundary condition in the flow solver requires no modification during the design cycle. The methodology can therefore be readily implemented with another existing explicit flow solver. In this paper, we make another original contribution where tip-leakage flow is included in the flow solution for the design procedure. As an example, the well-known NASA Rotor 67 transonic fan blade is chosen to illustrate the methodology.

2. Description of the Euler flow solver: analysis and design mode

Finite volume analysis of the three-dimensional unsteady Euler equations is used. The unsteady flow equations are discretized with respect to the cylindrical polar coordinates (r,θ,z) and are solved for steady solution.

Viscous effects are included using the log-law and mixing length models (descriptions in the next section) and the effect of blade rotation is also modelled. The developed solver uses a cell-vertex [22] approach and adopted central difference scheme with added dissipation and a multi-stage Runge-Kutta integrator [23]. Local time-stepping and grid sequencing have been implemented in the present computer code to accelerate convergence.

2.1. Modeling of viscous effects

The motivation to include viscous effects in Euler solutions stems directly from the fact that the computation of full Navier Stokes solution in an iterative fashion, as in an inverse design cycle, is expensive. It is risky to completely neglect the viscous effects, thus the inclusion of dissipative forces in inviscid solution is not uncommon [24] proposed the possibility of simple modeling using body-force where the dissipative stresses are directly computed from the classical skin friction coefficient. Despite being completely empirical, the approximation leads to realistic results. Denton [25] reported an improved extension of the work where the viscous forces are computed using the mixing length model. The latter is implemented here to model viscous losses. It is acknowledged that the modeling of viscous effects in the solver described here is based entirely on the method proposed by Denton [25]. It is also noted that the method employed is intermediate between being fully viscous and inviscid where the surface flow is allowed to slip along the solid walls. The model produces many of the details of real viscous flows but is very economical in terms of the number of cells required to achieve reasonable flow resolution. These were the prime considerations in the development of the current design method.

2.2. Boundary conditions: flow analysis

In the cascade calculation, four different types of boundaries are required: inlet, outlet, solid walls and periodicity.

At the inlet, the total pressure and temperature profiles and two absolute flow directions in the streamwise and meridional plane are specified. The static pressure is extrapolated from the interior flow field domain, which is used in conjunction with the isentropic relation to calculate the density and velocity. At the downstream boundary, the exit static pressure is held fixed on the hub and the radial variation is obtained via the radial equilibrium conditions.

A periodic or a cyclic condition is imposed to model the symmetry of flow between each sector of the cascade. This condition is applied upstream of the leading-edge and downstream of the trailing-edge where the values at two corresponding points are set to be equal.

The solid surfaces of the blade including the shroud and hub walls are represented by imposing zero normal convective fluxes. The surface flow therefore satisfies the tangency condition and slips along the surfaces.

2.3. Tip-clearance flow model

A simple tip-clearance model proposed by [26] is adopted in the present calculation. As shown in Figure 1, the radial mesh spacing (a-c or b-d) of the computational cells adjacent to the tip is taken to be tip gap. In the flow calculation, the tip-leakage effect is approximately included by equating flow variables at a and b (c and d).

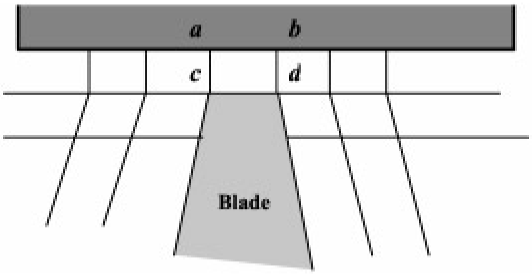

Figure 1. Periodic tip-leakage model

The current model is practical in terms of grid requirement. In addition, the model, although simple, is sufficient to represent the net effect of the tip clearance flow on the main flow. In the authors' experience, the current level of accuracy is adequate for the purpose of design and the simplicity of the model is a reasonably trade-off for computational speed. It is, however, noted that more sophisticated tip-leakage models may be readily applied with the proposed design principle if computational power and resources become a lesser constraint in routine design work.

2.4. Analysis validation

Validation of the present viscous flow solution has been made by calculating the steady flow through a transonic fan rotor, known as Rotor 67. This example is taken from the AGARD Report (AR275) entitled: *Test Cases for Computation of Internal Flows in Aero Engine Components* [27] catalogued specifically for validation of computational results. The experimental steady flow field has been extensively measured at NASA Lewis [28].

Rotor 67:

The flow of the transonic fan is highly three dimensional and viscous, and has been used by several researchers to verify their viscous solutions [26, 29, 30].

Vertical sheared H-grid topology is used to generate the computational domain which contains a total of 101 761 nodes; 29 points in the blade-to-blade direction, 121 points in the stream-wise direction with 63 points from the blade leading to trailing edge and 29 points in the span-wise direction from hub to shroud. The tip gap of about 0.8 percent is represented by the cells adjacent to the casing.

The flow computation is carried out under conditions corresponding to the rotor operating near its peak efficiency. The comparisons of total pressure, total temperature and flow angle at the rotor inlet (Aero Station 1) and/or outlet survey stations (Aero Station 2) with the experiments are shown in Figures 2, 3 and 4, respectively. As shown in Figure 2, along the exit survey station, good correlation of the total pressure ratio is observed.

There are also good comparisons of the total temperature ratio and the absolute exit swirl angle profiles. Figure 4 shows some overestimation in the prediction of the exit flow angle. This magnitude of difference is, however, in agreement with the results obtained by [26, 30]. In the figures, the corresponding result with no tip-leakage flow (open legend) may be compared. It is noted that while the fan blade has a tip-gap of only 0.8% blade height, a region of about 20% blade height near the tip is affected by the clearance flow (see solid legends).

As shown in Figure 5, the computed Mach number contours are also in close agreement with that obtained in the experiment using laser anemometry. Near the tip region, the transonic flow field interacts significantly with the tip leakage. The effect of the tip-leakage model used in the current computation is shown conclusively at the bottom plot of Figure 5 (90% blade height position). When no tip-leakage flow is modelled, the shock formation is significantly stronger. More importantly, the shock position is located further rear-ward. The discrepancies in the shock intensity and position in the flow prediction has a major effect when a re-design is carried out on the blade. This is illustrated in Section 4.2.

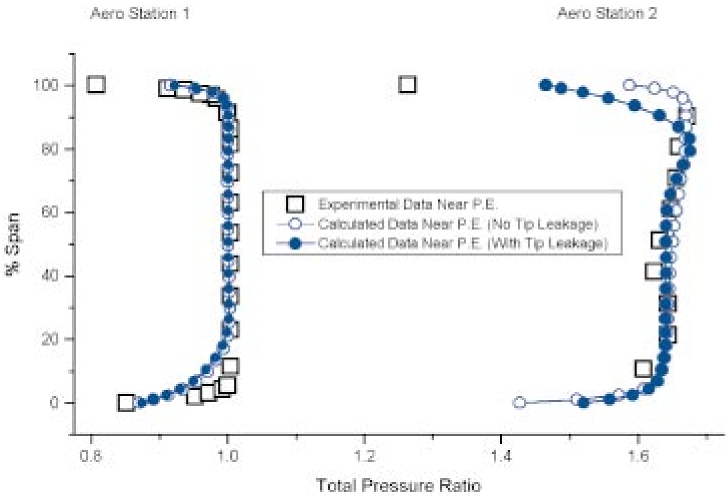

Figure 2. Total pressure profiles at Aero Station 1 and 2

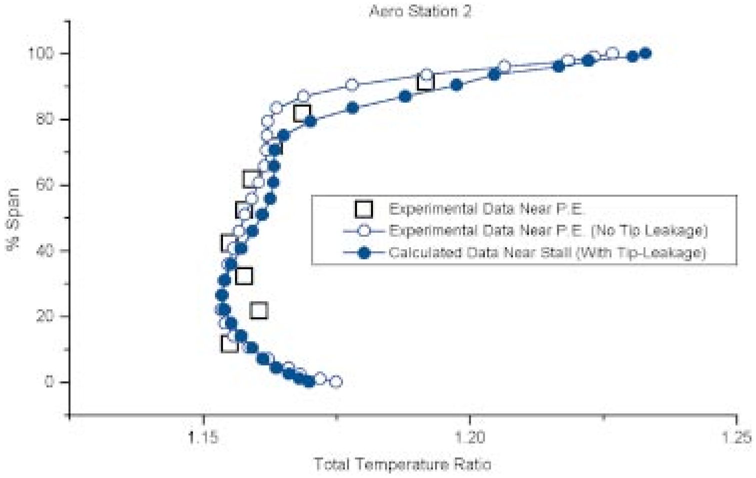

Figure 3. Total temperature profiles at Aero Station 2

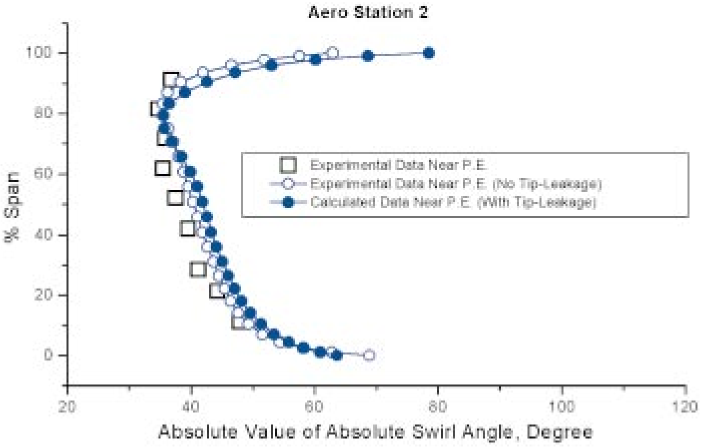

Figure 4. Swirl angle profiles at Aero Station 2

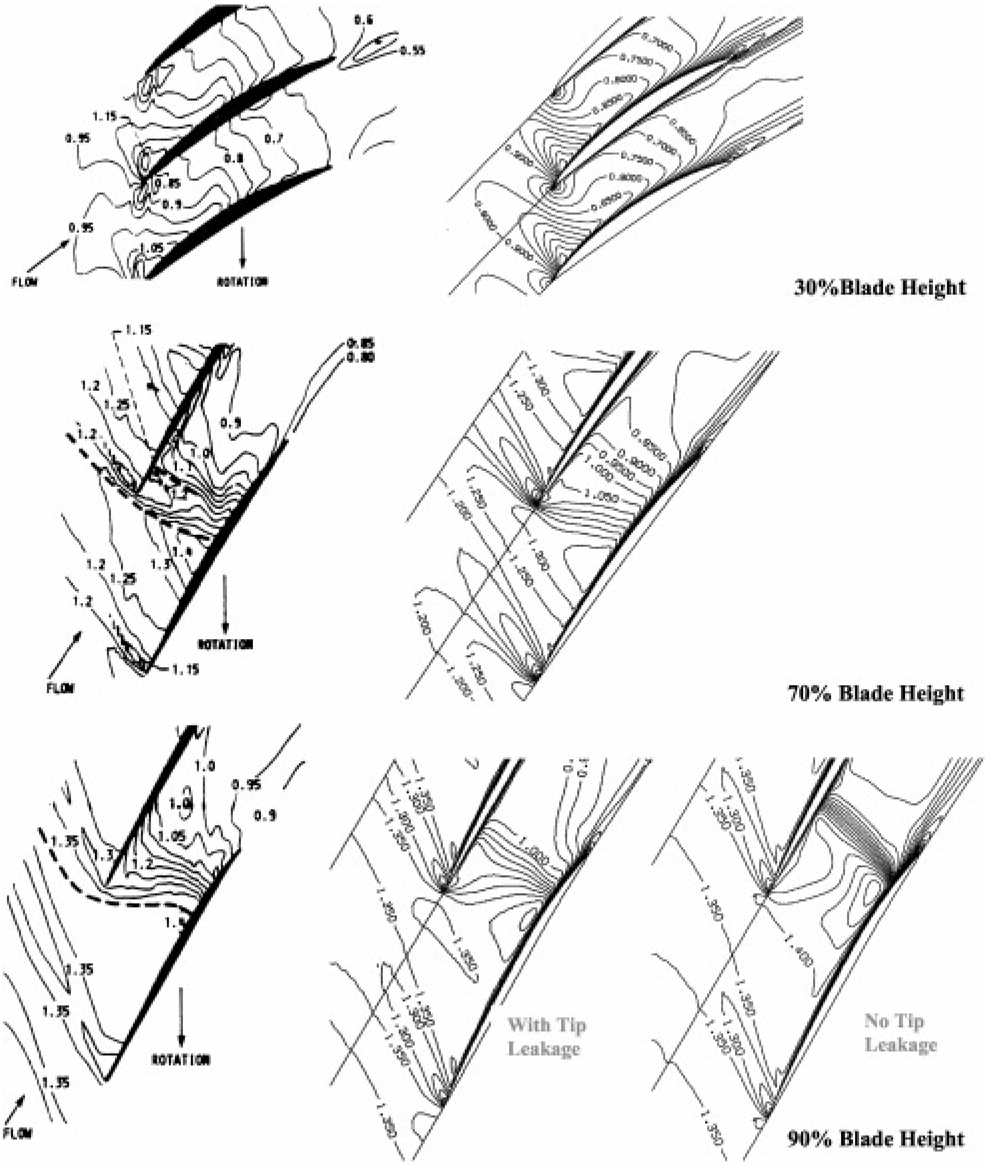

Figure 5. Experimental (left) and computed (right) contours of relative Mach number at the near-peak efficiency condition; contours at intervals of 0.05; dashed lines are estimated shock positions from [31]

3. Description of the inverse design method

In the inverse design procedure, the solver code and the blade design algorithm are coupled to form an automated design cycle. As illustrated in Figure 6, the essential steps are:

1. Input Initial blade geometry with fixed hub and casing surfaces;
2. Fix flow conditions in solver and calculate the steady flow solution;
3. Output the mass-averaged radius multiplied by tangential velocity $r\tilde{V}_\theta^0$;

4. Check if the target whirl velocity $r\tilde{V}_\theta^*$ is satisfied;
5. **If satisfactory**, final blade geometry has been obtained: output blade geometry and flow solution;

   If not, necessary blade modifications are calculated and the blade is updated. Process returns to step (2) and is repeated.

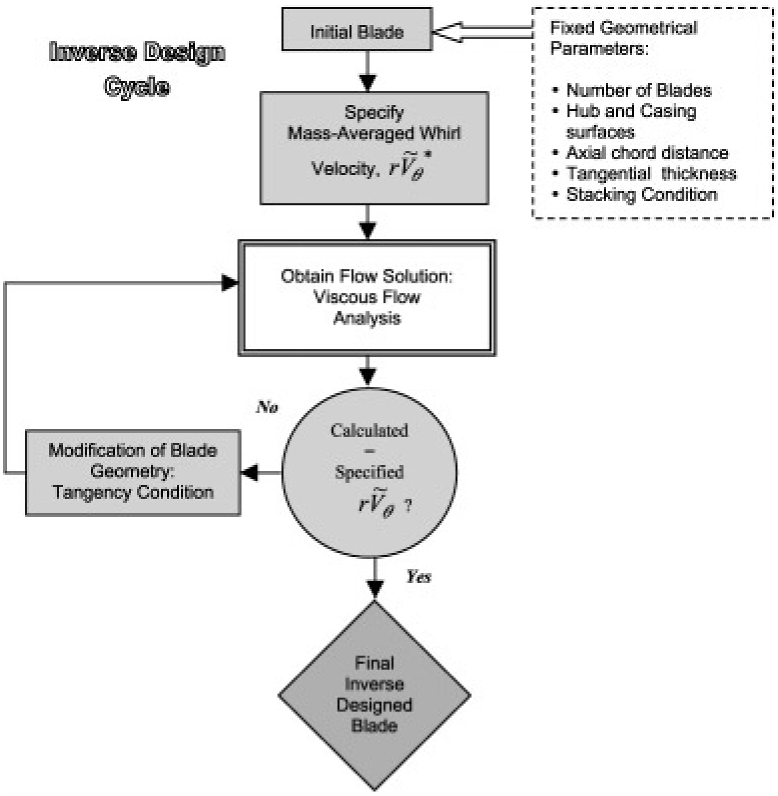

Figure 6. The proposed inverse procedure

3.1. Theoretical background of the design algorithm

As mentioned in Section 1, an important consideration in inverse methodology is the design specification. The current method makes use of average mean swirl (or whirl as it is also sometimes called) as the design specification. The background theory thus follows the work of [8–10] to which the reader is referred.

The prescribed quantity is the mass-averaged swirl quantity $r\tilde{V}_\theta$ and is defined as:

$$r\tilde{V}_\theta = \frac{\int_{SS}^{PS} rV_\theta(\rho V_m)d\theta}{\int_{SS}^{PS}(\rho V_m)d\theta}, \tag{1}$$

where PS and SS denote the pressure and suction sides of the blade, respectively. The specification of $r\tilde{V}_\theta$ is not arbitrary but is related to the specific work required by the machine through the turning of its blades. This relation is given by the Euler equation of turbomachinery which states,

$$W = \omega \left(r\tilde{V}_{\theta_{T.E.}} - r\tilde{V}_{\theta_{L.E.}} \right). \tag{2}$$

The rate of change of the averaged swirl velocity along the blade is also related to the static pressure difference $(P^+ - P^-)$ or ΔP across the blade. [8, 9] show that, within the assumption of an incompressible and irrotational flow, the pressure jump is related to the tangentially-averaged swirl velocity, *viz.*,

$$P^+ - P^- = \frac{2\pi}{N} \rho V_{mbl} \frac{\partial r\overline{V}_\theta}{\partial m}, \tag{3}$$

where V_{mbl} is the averaged meridional velocity across the blade and $\frac{\partial r\overline{V}_\theta}{\partial m}$ is the meridional derivative of the tangentially averaged swirl (In the current method, the mass-averaged swirl is used and its meridional derivative $\frac{\partial r\tilde{V}_\theta}{\partial m}$ is referred to here as the *Blade Loading*). Thus, advantages of using swirl velocity as the design parameter are twofold,

1. it allows design to be carried out directly based on the required work done, and
2. it allows control over the loading behavior of the blade.

Detailed formulation on how the target swirl $r\tilde{V}_\theta^*$ is used to calculate the corresponding blade geometry can be found in [18, 32]. The reader is referred to these publications.

3.2. Design specification

In the design procedure, the target $r\tilde{V}_\theta$ distribution is specified for the entire bladed meridional plane. A versatile way of defining the target design distribution is adopted from [33]. The basic approach to specifying the design specification in 3D is to select optimum distributions of $r\tilde{V}_\theta$ at the hub and shroud and linearly interpolate the values to generate the overall distribution on the whole of the meridional plane.

Equation (3) shows the relation of the surface pressure to the $\frac{\partial r V_\theta}{\partial m}$ (or loading distribution), therefore by specifying a smooth blade loading distribution, it is also possible to ensure smooth surface pressure variations. All these criteria are found to be more easily satisfied by specifying the loading distribution rather than the $r\tilde{V}_\theta$ distribution.

3.3. Design with tip gap

In the design of the blade with tip-leakage gap, the use of linearly interpolated $r\tilde{V}_\theta$ design specification from the hub to tip may not be adequate resulting in unrealistic shape of the tip section. In the current implementation, the user is also allowed to select a proportion of the blade tip where the geometry is defined by extrapolating radially the geometry computed from within.

3.4. Convergence criterion

During the design cycle, the difference in swirl $(r\tilde{V}_\theta^* - r\tilde{V}_\theta^n)$ is checked after each blade modification and the procedure is completed when the tolerance becomes sufficiently small. A typical value of 1% match with the specification is generally found to be adequate for the typical application. This is demonstrated in the next section.

4. Results

4.1. Validation: reproducing the fan blade

The computed $r\tilde{V}_\theta$ distribution across the entire meridional plane of the original Rotor 67 fan is shown in Figure 7. For the validation, the original $r\tilde{V}_\theta$ distribution is imposed as the design specification in the design code and the objective is to reproduce the original blade starting with a different geometry.

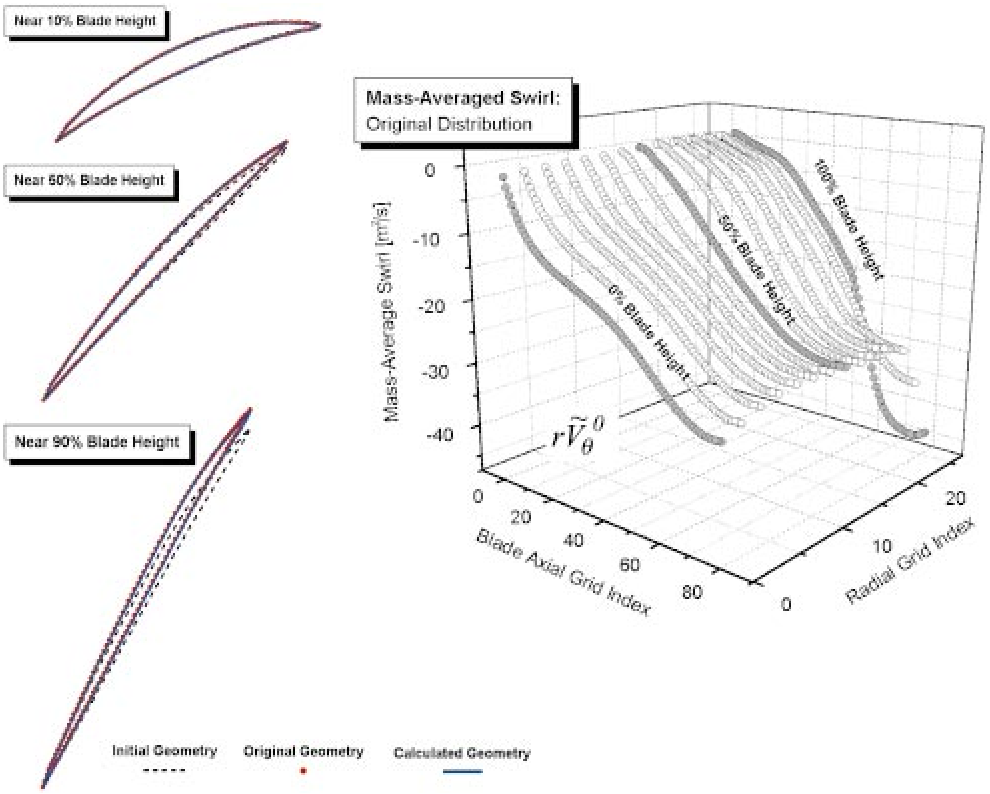

Figure 7. Validation of the inverse methodology: target loading distributions and reproducing the fan blade

The left of the figure shows the final result of the computation where the blade shapes are compared at three blade heights; near the hub, at mid-span and near the tip. In each of the three plots, the initial (dashed line), the target (solid line) and the final profile (dots) are shown. At all three span positions, the reproduced geometry matches the original shape closely. The results therefore verify the accuracy of the algorithm.

4.2. Re-design of NASA Rotor 67

Modifications to the original Rotor 67 fan blade are made using the present procedure. The blade loading, $\frac{\partial r\tilde{V}_\theta}{\partial m}$, distribution of the original blade and the relative Mach number contours at three blade heights are shown in Figure 8. It is noted that near the tip region where there is a shock formation across the passage and interaction with the leakage flow, the blade loading, shows large variation. Also, in

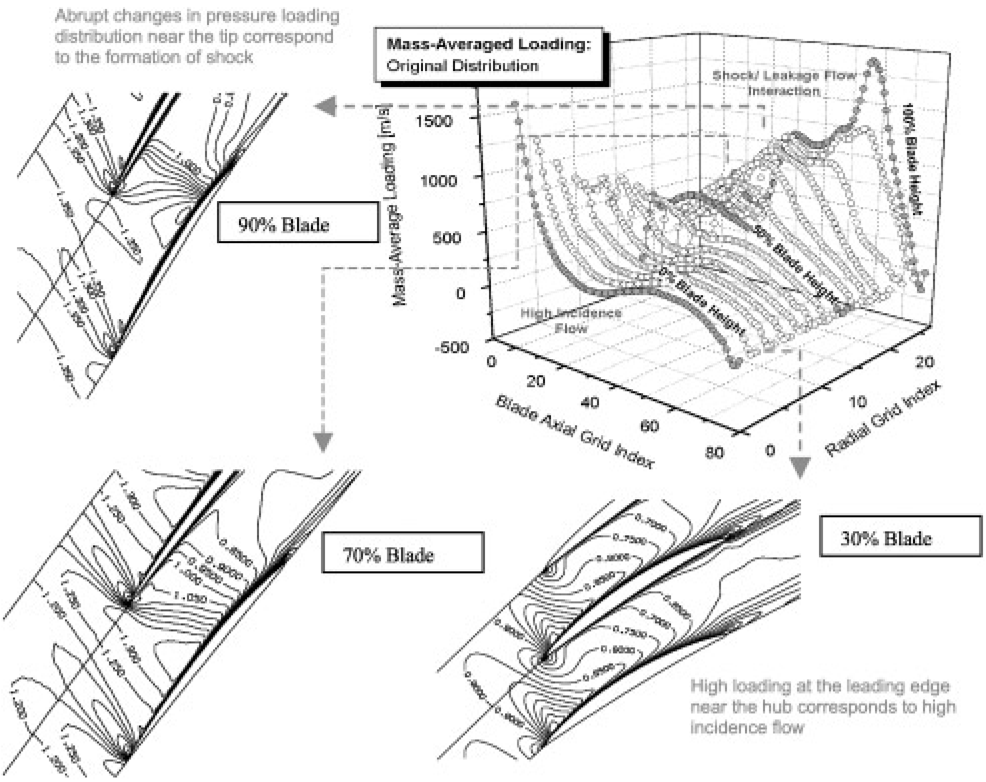

Figure 8. Original blade loading distribution (with relative Mach number contours at three blade heights)

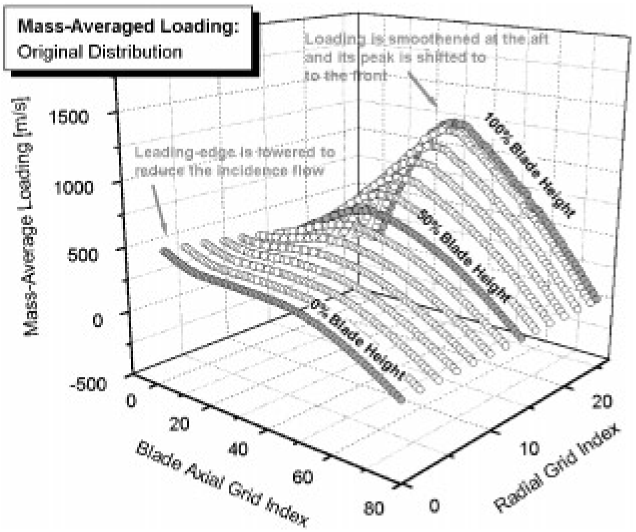

Figure 9. Specified loading distribution for the re-design of the rotor

the region near the hub, the high flow incidence is reflected by the high leading-edge loading. The re-design therefore concentrates on improving these two areas of the blade aerodynamics.

To illustrate the methodology, the re-design is specified to affect the shock formation near the tip by adopting a moderately fore-loaded characteristic. Along the hub, the leading-edge loading is lowered to control the incidence flow. The distribution of the design blade loading specification is shown in Figure 9.

4.3. Overview of the aerodynamics changes

4.3.1. High flow incidence at the hub

The main undesirable flow phenomenon near the hub region of the original blade is the presence of flow re-circulation at the inlet (see top left hand side plot in Figure 10).

This is a direct consequence of having a highly loaded inlet region, which in terms of the flow aerodynamics, gives rise to a high incidence flow near the hub of the blade. The re-design reduces the high positive incidence flow directly by alleviating the load through a decreased $\frac{\partial r\tilde{V}_\theta}{\partial m}$ value at the leading edge. As can be seen in Figure 10, suppression of the incidence induced separation immediately achieved.

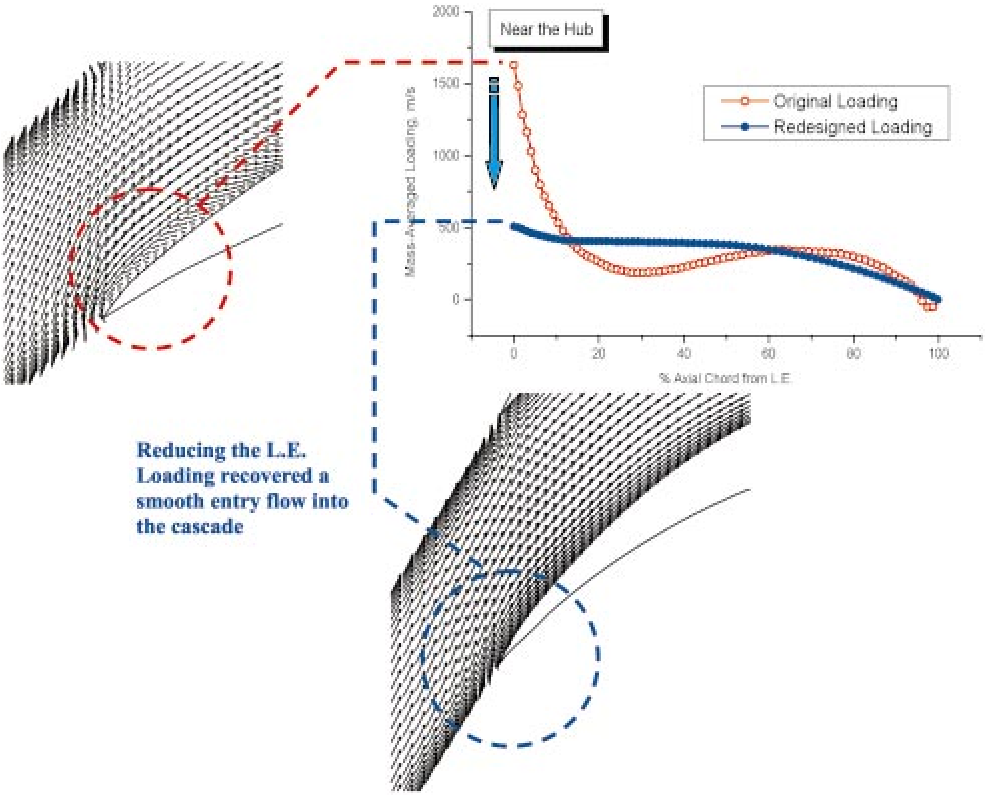

Reducing the L.E. Loading recovered a smooth entry flow into the cascade

Figure 10. Mass-averaged loading distributions with corresponding relative velocity vectors at the hub: original and re-design

4.3.2. Mach number and shock formation

Near the blade tip, the flow aerodynamics present a different design focus. Here, the flow is predominantly transonic and the interaction with the tip-leakage flow is highly complex. For the purpose of illustrating the methodology, the re-design aims only to shift the shock position by controlling the $\frac{\partial r\tilde{V}_\theta}{\partial m}$ distribution.

At 90% blade height position, it is interesting to note that the effects of the shock are registered separately on the mass-averaged loading distribution (see rightmost plot of Figure 11); the first peak in $\frac{\partial r\tilde{V}_\theta}{\partial m}$ corresponds to the shock on the pressure side and the second, that on the suction side of the blade.

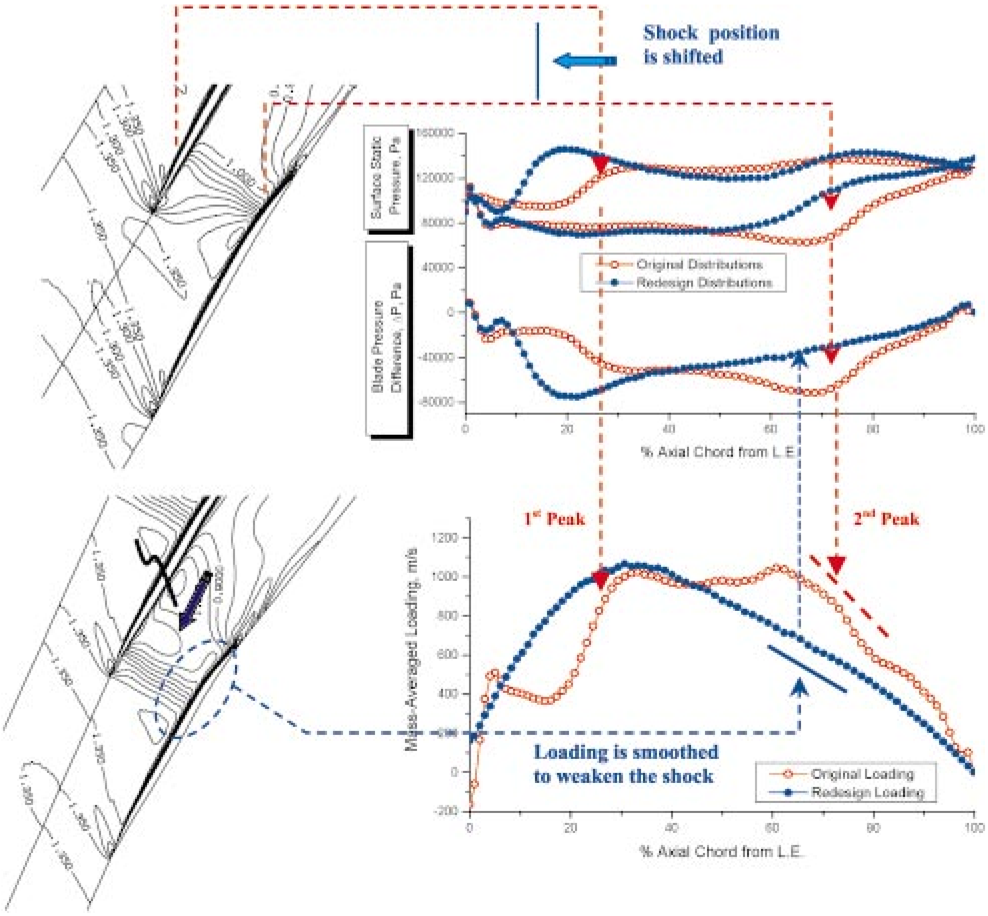

Figure 11. Relative Mach number contours at 90% blade height: original and re-design (showing relationships to the static pressure distributions and $\frac{\partial r\tilde{V}_\theta}{\partial m}$)

In the re-design, the loading at the front is increased to give a smoothed but completely fore-loaded characteristic at the tip. The relocation of the loading peak towards the front shifts the pressure leg of the shock towards the front. At the rear half of the blade, the abrupt variation of the loading corresponding to the suction leg of the original shock is replaced by a smooth variation. The result of this specification gives rise to overall smoother surface pressure distribution at the rear. This corresponds to the pressure leg of the shock formation being weakened, which may be observed as the diffused Mach number contours shown in the bottom left hand plot of Figure 11.

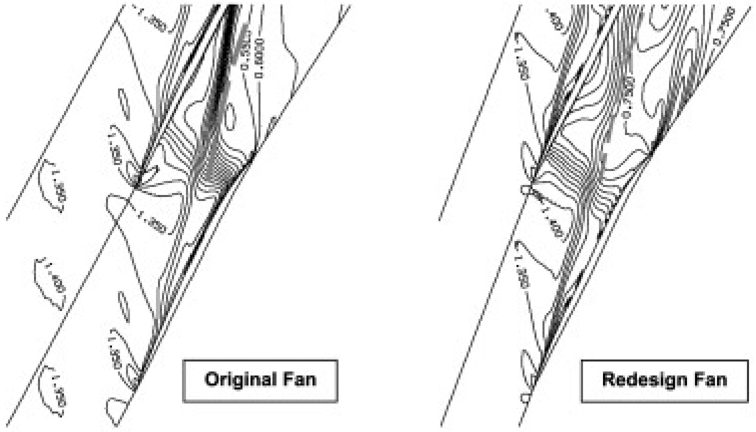

Figure 12. Relative Mach number contours at blade tip: original and re-design (contour interval: 0.05)

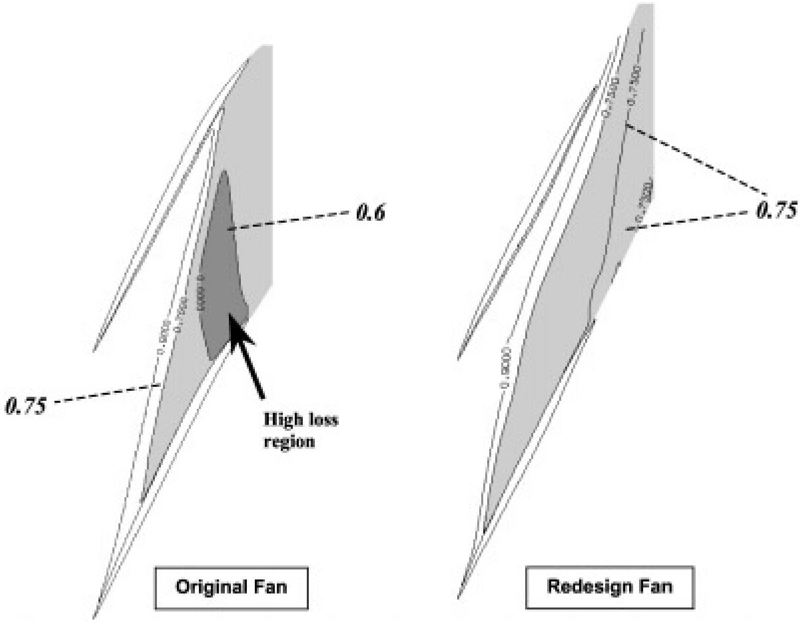

Figure 13. Contours of entropy generation, $\exp(-\Delta S/R)$ at the blade tip: original and re-design (contour interval: 0.15)

As shown in Equation (3) of Section 3.1, $\frac{\partial r V_\theta}{\partial m}$ is directly proportional to the pressure loading, ΔP across the blade. This relation is illustrated between the distribution of ΔP shown on the top right-hand plot and the bottom plot showing the $\frac{\partial r \bar{V}_\theta}{\partial m}$ values. This correspondence forms the main mechanism that allows the current design specification to affect the surface aerodynamics of a design (which traditionally was controlled only by affecting surface pressure or velocity distributions).

At the blade tip, the flow field exhibits complex shock-boundary layer and tip-leakage flow interactions. Figure 12 shows the blade-to-blade Mach number contours of the blade profile at the tip (*i.e.* 100% blade height). With the re-design, the interaction seemingly becomes less severe as a result of an overall weaker shock formation in the tip region. While it is difficult to quantify separately the losses due to the shock-boundary layer and leakage flow, the generated entropy gives a qualitative measure of the overall loss as a result of the re-design. This is shown in Figure 13 where the region of high entropy generation (shaded in darker grey) may be compared between the original and new designs. The contours are values of $\exp(-\Delta S/R)$ where the value of 1.0 represents no thermodynamic irreversibilities and decreases when the loss is higher. As may be observed, there is a substantial reduction of high loss region in the new design.

The concentration of entropy generation along the trailing edges across the entire span is shown in Figure 14. As depicted, the most significant improvement of the new design is a one and a quarter point reduction of the overall mass-averaged entropy generation/loss in the region near the blade tip.

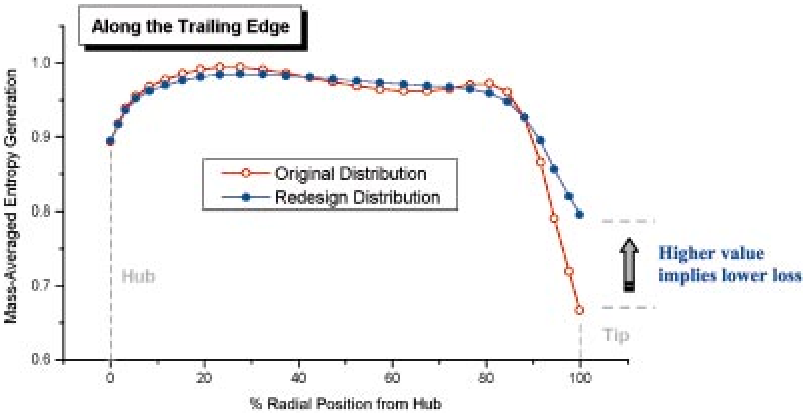

Figure 14. Radial distribution of the mass-averaged $\exp(-\Delta S/R)$ at the trailing edge: original and re-design

5. Concluding remarks

The development and application of a 3D inverse method is presented for the design of unshrouded turbomachinery (with tip-gap) blades. The method solves for the blade geometry based on the specification of the mass-averaged swirl velocity $r\tilde{V}_\theta$ and a fixed tangential thickness distribution. The flow model is based on a 3D time-marching viscous solver where a tip-leakage model is included in the implementation. The net effect of the tip flow on the overall flow is therefore included throughout the design process.

The proposed methodology was validated using the NASA Lewis Rotor 67 based on the specification of its swirl velocity distribution but starting from a different geometry. To further illustrate the design methodology, the design method was applied to re-design the transonic fan blade. Design efforts concentrated on improving the poor incidence near the hub and affecting the shock formation near the tip by changing the loading $\frac{\partial r\tilde{V}_\theta}{\partial m}$ characteristics. An observed improvement in the flow aerodynamics was made. Further practical applications of the current method are scheduled to be carried out in the near future.

Acknowledgements

The authors are thankful to Ebara Research Co. LTD. for providing financial and technical support to the work presented. Thanks are particularly due to Dr. Akira Goto, Dr. Hideomi Harada and Mr. Hiroyoshi Watanabe for sharing their expertise and making many useful suggestions over the course of the current work.

References

[1] Casey M V 1994 *AGARD LS* **195**, *Turbomachinery Design Using CFD*

[2] Demeulenaere A and Van den Braembussche R A 1996 *ASME Paper* **96-GT-39**

[3] Dulikravich G S and Baker D P 1999 *AIAA Paper* **99-0185**

[4] Wang Z, Cai R, Chen H and Zhang D A 1998 *ASME Paper* **98-GT-126**

[5] Dang T 1995 *AIAA Paper* **95-2465**

[6] Ahmadi M and Ghaly W S 1997 *Proc. 5th Conf. CFD Society of Canada* **CFD-97** 2-15-2-21

[7] Tiow W T and Zangeneh M 1998 *ASME Paper* **98-GT-125**

[8] Hawthorne W R, Tan C S, Wang C and McCune J 1984 *J. Eng. for Gas Turbines and Power* **106** 346

[9] Tan C S, Hawthorne W R, McCune J E and Wang C 1984 *J. Eng. for Gas Turbines and Power* **106** 355

[10] Zangeneh M 1991 *Int. J. Numerical Methods in Fluids* **13** 599

[11] Leonard O and Van den Braembussche R A 1991 *ASME Paper* **91-GT-18**

[12] Goto A and Zangeneh M 1998 *ASME Paper* **FEDSM98-4854**

[13] Zangeneh M, Goto A and Harada H 1998 *ASME J. Turbomachinery* **120** 723

[14] Ashihara K and Goto A 1999 *ASME Paper* **FEDSM99-6846**

[15] Watanabe H and Harada H 1999 *ASME Paper* **99-GT-72**

[16] Demeulenaere A, Leonard O and Van den Braembussche R A 1997 *Proc. Inst. Mech. Engrs., Part A, J. Power and Energy* **211** 299

[17] Damle S V 1998 *Fully Three-Dimensional and Viscous Inverse Method for Turbomachinery Blade Design*, PhD Thesis, Department of Mechanical Engineering, Syracuse University

[18] Tiow W T 2000 *Inverse Design of Turbomachinery Blades in Rotational Flow*, PhD Thesis, University College, University of London

[19] Damle S and Dang T 1998 *ASME Paper* **98-GT-115**

[20] Tiow W T and Zangeneh M 2001 *Proc. IMechE Symp. Advances of CFD in Fluid Machinery Design*

[21] Qiu X and Dang T 2000 *ASME Paper* **2000-GT-0526**

[22] Hall M G 1986 *Proc. Conf. on Numerical Methods for Fluid Dynamics*, eds. Morton K W and Baines M J, Reading, UK, pp. 303–345

[23] Jameson A, Schmidt W and Turkel E 1981 *AIAA Paper* **81-1259**

[24] Denton J D 1986 *ASME Paper* **86-GT-144**

[25] Denton J D 1990 *ASME Paper* **90-GT-19**

[26] He L and Denton J D 1994 *ASME J. Turbomachinery* **116** 469

[27] AGARD-AR-275 1985 *Test Cases for Computation of Internal Flows in Aero Engine Components*

[28] Strazisar A J, Wood J R, Hathaway M D and Suder K L 1989 *NASA Technical Paper* 2879

[29] Jennions I K and Turner M G 1993 *ASME J. Turbomachinery* **115** 261

[30] Arnone A 1994 *ASME J. Turbomachinery* **116** 435

[31] Pierzga M J and Wood J R 1985 *ASME J. Engineering for Gas Turbines and Power* **107** 436

[32] Tiow W T and Zangeneh M 2000 *ASME Paper* **2000-GT-525**

[33] Zangeneh M, Goto A and Takemura T 1996 *ASME J. Turbomachinery* **118** 536